Earth and Planetary Science Letters 274 (2008) 157–168

Contents lists available at ScienceDirect

Earth and Planetary Science Letters

journal homepage: www.elsevier.com/locate/epsl

Subduction of the Indian lithosphere beneath the Tibetan Plateau and Burma

Chang Li [a,*], Robert D. van der Hilst [a], Anne S. Meltzer [b], E. Robert Engdahl [c]

[a] Department of Earth, Atmospheric, and Planetary Sciences, Massachusetts Institute of Technology, 77 Massachusetts Ave., Cambridge, MA 02139, USA
[b] Earth and Environmental Sciences, Lehigh University, 31 Williams Drive, Bethlehem, PA 18015, USA
[c] Department of Physics, University of Colorado, Campus Box 390, Boulder, CO 80309-0390, USA

ARTICLE INFO

Article history:
Received 8 August 2007
Received in revised form 7 July 2008
Accepted 10 July 2008
Available online 20 July 2008

Editor: C.P. Jaupart

Keywords:
Indian subduction
Tibetan plateau
Burma
upper mantle
travel time tomography

ABSTRACT

Subduction of the Indian lithosphere under Eurasia plays an important role in the tectonic evolution of the Tibetan plateau and surrounding regions. To improve our knowledge of pertinent mantle structures through tomographic imaging we combine *P*-wave arrival time data from temporary arrays in Tibet and stations of the Chinese Seismograph Network with reprocessed data from the International Seismological Centre. The new images reveal considerable spatial variations in mantle structure along the collision zone, and the horizontal distance over which presumed (continental) Indian lithosphere slides northward beneath the plateau decreases from west (where it underlies the Himalayas and the entire plateau) to east (where no indication is found for present-day underthrusting beyond the Himalayan Block and Indus–Tsangpo suture). *P*-wavespeed appears low in the shallow mantle beneath much of central and eastern Tibet. These observations suggest that Indian lithosphere underlies only the southwestern part of the plateau and that the central and northeastern part is underlain by lithosphere of Asian origin. The (continental) parts of the Indian plate that currently underthrust or subduct below the plateau appear generally detached from the (oceanic) slab fragments that subducted longer ago and that have been detected deeper in the mantle, except perhaps in the central part of the collision zone (80–90°E). This suggests that ongoing India–Eurasia collision must increasingly be driven by other forces, such as subduction of the Indian plate further west and east (e.g. beneath Indochina). Our images reveal structures associated with eastward subduction along the Burmese arc southeast of the eastern Himalayan syntaxis. The Tengchong volcanic complex in southwest China is marked by slow wave propagation to ~150 km depth, suggesting a causal link to subduction along the Burmese arc; the low velocities beneath the Red River fault region extend to greater depth and may be related to upper mantle processes further southeast.

1. Introduction

The Tibetan plateau, with an elevation of 4–5 km above sea level and underlain by crust of ~70 km thick, was generated by the collision and post-collisional intra-continental deformation of Indian and Eurasian plates beginning ~50 Myr ago (e.g., Argand, 1924; Molnar and Tapponnier, 1975; Yin and Harrison, 2000).

From geology and (kinematic) plate reconstructions (e.g., Besse and Courtillot, 1988; Lee and Lawver, 1995), the post-collision convergence between the Indian and Eurasian plates is estimated to be at least 1000–1400 km (Yin and Harrison, 2000) but perhaps as much as 2000–3000 km (Molnar et al., 1993; Rowley, 1998). How this shortening has been accommodated is still not well known and several scenarios have been proposed for the tectonic evolution of Tibet. These include uniform thickening and shorting of Asian lithosphere (England and Houseman, 1986; Dewey et al., 1988), block extrusion along major strike-slip faults (Tapponnier et al., 1982, 2001), southward subduction of Asian lithosphere under Tibet (Willett and Beaumont, 1994; Kind et al., 2002), and thrusting of the Indian lithospheric mantle under much (or all) of the plateau (e.g., Argand, 1924; Ni and Barazangi, 1984; Powell, 1986; Holt and Wallace, 1990; Owens and Zandt, 1997).

There is no doubt that subduction of the Indian plate beneath Asia has played a key role in the tectonic evolution of Tibet. Late Mesozoic and early Cenozoic subduction of the Tethys ocean floor deep into Earth's mantle has been reconstructed from seismic tomography and plate reconstructions (Van der Voo et al., 1999; Replumaz et al., 2004; Hafkenscheid et al., 2006) but the structure of the upper mantle beneath Tibet has not been resolved in sufficient detail to understand the transition from ancient subduction of oceanic lithosphere to the more recent subduction of (presumably) continental lithosphere. Consequently, even first-order questions have remained unanswered.

Seismic tomography has not yet provided unequivocal constraints on the (present day) northward extent of the Indian lithosphere underneath the plateau. Some surface wave studies reveal fast wave propagation beneath much of Tibet (e.g., Shapiro and Ritzwoller,

* Corresponding author. Tel.: +1 617 324 0268; fax: +1 617 258 9697.
E-mail address: changli007@gmail.com (C. Li).

0012-821X/$ – see front matter © 2008 Elsevier B.V. All rights reserved.
doi:10.1016/j.epsl.2008.07.016

2002), and Priestley et al. (2006) suggest that the entire plateau is underlain by a relatively cold lithospheric mantle (to 225–250 km depth). From *P*-wave (travel time) tomography Zhou and Murphy (2005) argue that the Indian plate underthrusts across the entire plateau. Other studies report low upper-mantle *S* velocities beneath the northern and central plateau (Brandon and Romanowicz, 1986; Griot et al., 1998; Friederich, 2003; Raphine et al., 2003; Lebedev and van der Hilst, 2008), which is consistent with inefficient *Sn* propagation and low *Pn* velocities in the north (Barazangi and Ni, 1982; McNamara et al., 1995, 1997). Curtis and Woodhouse (1997) conclude that regional surface wave dispersion is inconsistent with large scale underthrusting of Indian lithosphere beneath the plateau unless the plate is chemically altered or thin (<85 km).

The INDEPTH project (Nelson et al., 1996) enabled high-resolution imaging of the crust and upper mantle beneath central Tibet. Zhao et al. (1993) showed that intact (continental) Indian lithosphere underthrusts the Himalayas. Further north, however, the fate of this lithosphere is ambiguous. Tilmann et al. (2003) argue that it underthrusts the plateau as far as the Bangong–Nujiang suture, central Tibet (Fig. 1), from where it may sink sub-vertically to at least 400 km depth (Fig. 2a). In contrast, Kosarev et al. (1999) suggest that Indian lithosphere plunges northward near the Indus–Tsangpo (or Indus–Yarlung or Yarlung–Zangbo) suture (Fig. 1) and is detached from the surface beneath central Tibet (Fig. 2b).

Some of the differences in interpretation may reflect ambiguities resulting from 2-D sampling (along the linear INDEPTH arrays) of complex 3-D mantle heterogeneity. To increase 3-D data coverage, MIT and Lehigh University, in collaboration with the Chengdu Institute of Geology and Mineral Resources (CIGMR), deployed broad-band seismograph arrays in southeastern Tibet. Data from these deployments has previously been used for high-resolution surface-wave array tomography (Yao et al., 2006, 2008), crustal studies with receiver functions (Xu et al., 2007), and to study anisotropy with shear-wave splitting (Lev et al., 2006; Sol et al., 2007). Here we present tomographic images of 3-D upper mantle heterogeneity beneath Tibet and surrounding regions obtained from travel time tomography with data from these MIT and Lehigh arrays as well as from other temporary arrays in the region (including INDEPTH) and the Chinese Seismograph Network. In total, we used travel time data from nearly 1500 seismograph stations in and near mainland China (Fig. 3), and we inverted these data along with the global data base from the International Seismological Centre (ISC), as reprocessed by Engdahl et al. (1998).

The images inferred from the combined data sets reveal significant lateral variations in subduction-related mantle structure beneath the collision zone and suggest that the horizontal distance over which the Indian lithosphere slides northward beneath the plateau decreases from west (where it underlies the Himalayas and the entire plateau) to east (where no indication is found for underthrusting beyond the Himalayan Block). Except perhaps in the center of the collision zone, the (continental) parts of the Indian plate that currently underthrust or subduct below the plateau appear detached from the (oceanic) slab fragments detected deeper in the mantle. In addition to these first-order results, we also describe the mantle structure pertaining to subduction southeast of the eastern Himalayan syntaxis, along the Burmese arc.

2. New data sets for seismic tomography

We use *P*-wave travel time data from three principal sources: (1) regional (temporary) seismic arrays in Tibet and nearby area; (2) national and provincial stations of the Chinese Seismograph Network (CSN); and (3) the global EHB data base (Engdahl et al., 1998). These data are inverted along with a global data set of ~22,000 differential travel time residuals of *PP-P*, which helps constrain the upper mantle structure beneath regions with few earthquakes and stations (e.g., western Tibet and Tarim Basin).

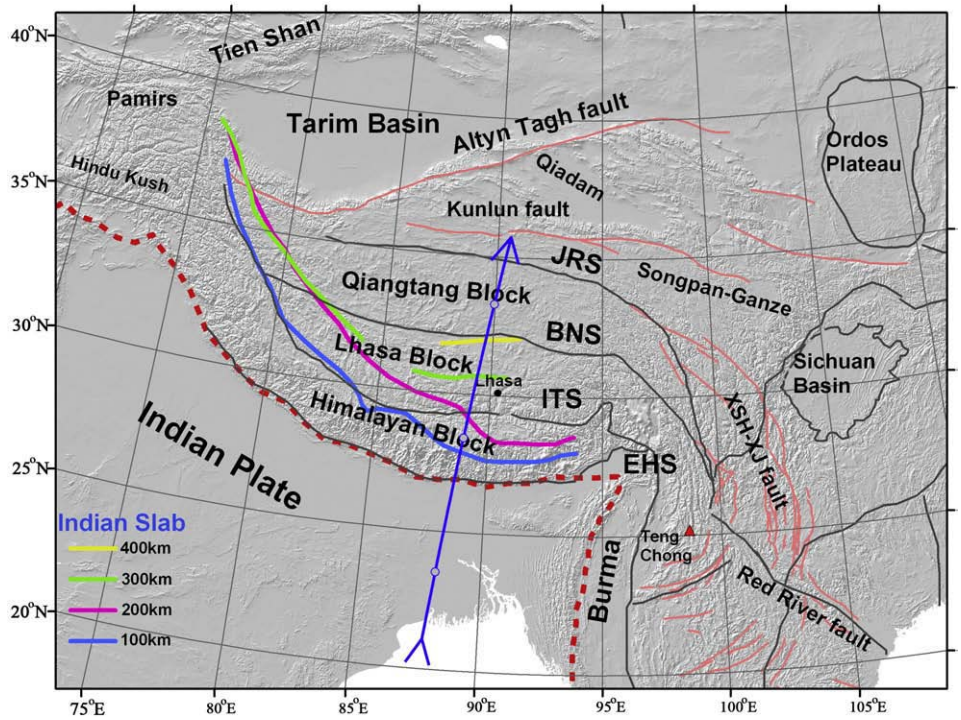

Fig. 1. Map of study region, including depth contours of the Indian plate beneath the Tibetan plateau inferred from tomography. The background shows topography (grey) and strike-slip faults (pink lines) around Tibet. Grey lines represent the tectonic boundaries and sutures, where ITS — Indus–Tsangpo suture, BNS — Bangong–Nujiang suture, JRS — Jinsha River suture (Tapponnier et al., 2001). Dashed red lines are the plate boundaries, according to NUVEL-1 (DeMets et al., 1990). Red triangle (98°E, 25°N) is the center of the Tengchong volcanic complex. The blue arrow marks the location of the cross section shown in Fig. 2. (For interpretation of the references to colour in this figure legend, the reader is referred to the web version of this article.)

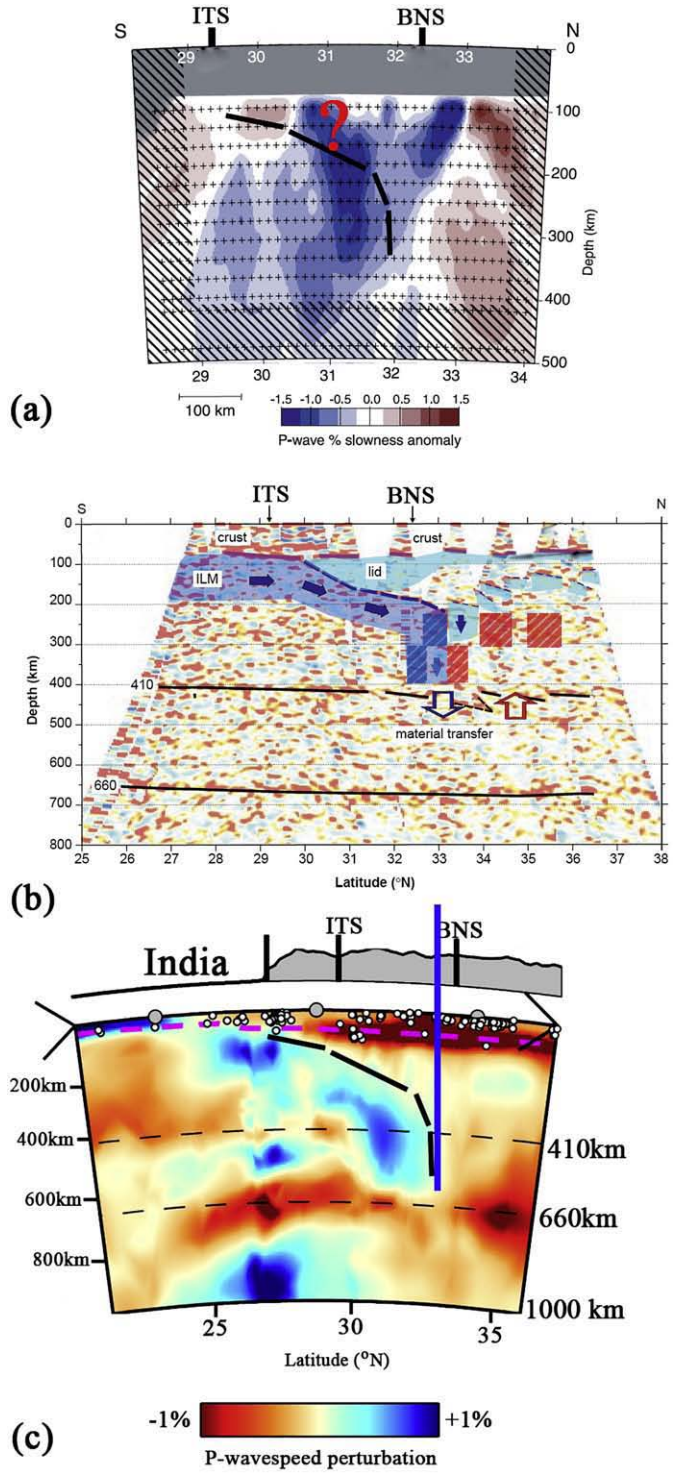

Fig. 2. Comparison with seismic imaging studies from INDEPTH projects beneath central Tibet (in the range of [87°E, 90°E] and [29°N, 34°N]). (a) Teleseismic tomography based on the INDEPTH II and III data (Tilmann et al., 2003); (b) Teleseismic receiver function image from the INDEPTH II and Sino-American PASSCAL experiments (Kosarev et al., 1999); (c) this study (location of this cross section is depicted in Fig. 1), where the blue line shows the northern foremost edge of the subducted Indian plate. (For interpretation of the references to colour in this figure legend, the reader is referred to the web version of this article.)

2.1. Regional array data

To improve the resolution of mantle structure beneath Tibet we picked *P*-wave arrivals from local, regional, and teleseismic earthquakes recorded at ~170 seismograph stations of the MIT-CIGMR, Lehigh-CIGMR, and several previous seismic arrays on the plateau (blue symbols in Fig. 3). Since the size of these datasets prohibits manual processing we used an automated phase picker (Aldersons et al., 2003). To calibrate (or 'train') the algorithm to our specific data, we manually picked ~20% of the raw data and used comparisons with automatic picks to tune the picking engine and ensure accuracy and consistency. In total, we obtained ~35,000 *P* arrivals from the temporary array deployments.

2.2. Chinese Seismograph Network (CSN)

From ~1000 national and regional stations of the CSN (red squares on Fig. 3) we used about 1 million *P* phases from earthquakes occurring between 1967 to 2004, which far exceed (but include) the data from the Annual Bulletin of Chinese Earthquake (ABCE) used before (e.g., Li et al., 2006).

2.3. Global data

From the global data processed by Engdahl et al. (1998), hereinafter referred to as EHB data, we use ~12 million *P*, *Pg*, *pP*, *Pn* and *PKP* phases from 1964 to 2007. In EHB, by convention, *Pn* refers to *P* phases with turning points less than 410 km; to select turning rays and discard post-critical 'head waves' we require either that the focal depth is larger than 80 km or that the turning point is deeper than 100 km. In our study region most EHB stations (yellow triangles in Fig. 3) are located on the Indian plate, along the Himalayas, and in Kyrgyzstan. This data has been described in detail by Engdahl et al. (1998) and Li et al. (2006, 2008) and is not discussed further here.

Careful processing is required to combine the data from these sources into an internally consistent data base for tomography. We first associate the arrival times from each dataset with the corresponding events. Duplicate stations, for which arrival time data are reported in more than one of the datasets, are then subjected to special examination: obvious errors are discarded but if we have no reason to reject one of them we treat both readings as independent data. This concerns only a very tiny subset of the data, however. Finally, to insure that all of the travel time data are internally consistent we relocate each event with the combined arrival time data using a non-linear process of earthquake relocation and phase re-identification (Engdahl et al., 1998) to produce new travel time residuals with respect to the new computed hypocenter. To compensate for the relatively small volume but high quality of the datasets compared to the routinely processed global and regional data, however, we apply larger weights to data from the Tibetan arrays.

The arrays represent a significant increase of data coverage on the plateau and surrounding areas. In Fig. 4 we show travel time residuals (computed by subtracting travel times calculated from the *ak135* reference model, Kennett et al. (1995), and after elevation correction) at each station as a function of back-azimuth. For most of these stations we have more than 200 picks. The mean (positive) delay of ~2 s reflects the thick Tibetan crust, which we account for upon inversion (see below). The residuals show distinct direction dependence. For all stations, arrivals from earthquakes north and northwest of the arrays have large and positive residuals (that is, their travel times are larger than in reference model *ak135*). In contrast, most arrivals from the south and southeast appear relatively early. We assume that this pattern is a manifestation of mantle heterogeneity, with slow *P*-wave propagation beneath the plateau and higher propagation speed further south, but a contribution from large scale anisotropy cannot be excluded.

3. Multi-scale travel time tomography

We perform global inversions but by adapting the parameterization (by means of variable size 3-D blocks) to the sampling density (see Kárason and van der Hilst, 2000) we obtain high resolution in regions of

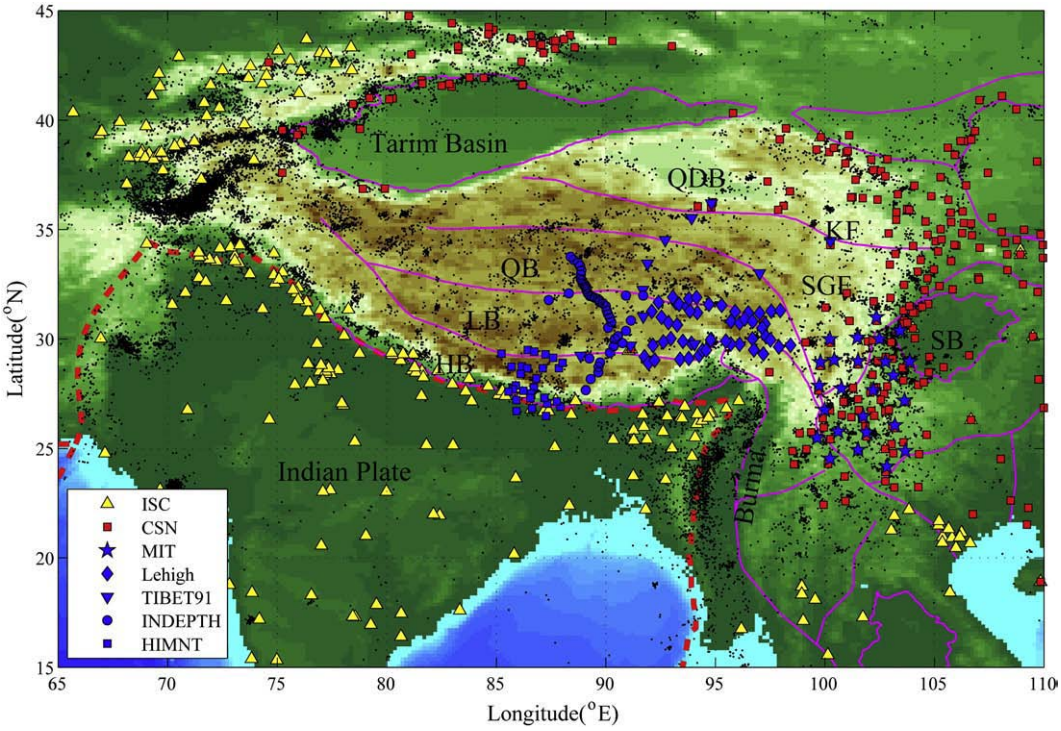

Fig. 3. Stations and events in Tibet and surrounding regions. The pink lines mark the tectonic block boundaries in the region, where QDB-Qaidam Basin, KF-Kunlun Fault, SB-Sichuan Basin, SGF-Songpan Ganze Foldbelt, QB-Qiangtang Block, LB-Lhasa Block, HB-Himalayan Block. The suture zones and plate boundaries are same as in Fig. 1. (For interpretation of the references to colour in this figure legend, the reader is referred to the web version of this article.)

particular interest (and with sufficient data coverage). The size of a block is a multiple of 45 km×0.35°×0.35° in depth, latitude, and longitude beneath the plateau and surrounding regions (down to 800 km depth) and 45 km×0.7°×0.7° elsewhere. The total number of free parameters (the sampled irregular blocks and the event relocation parameters in the global model) is about 0.5 million.

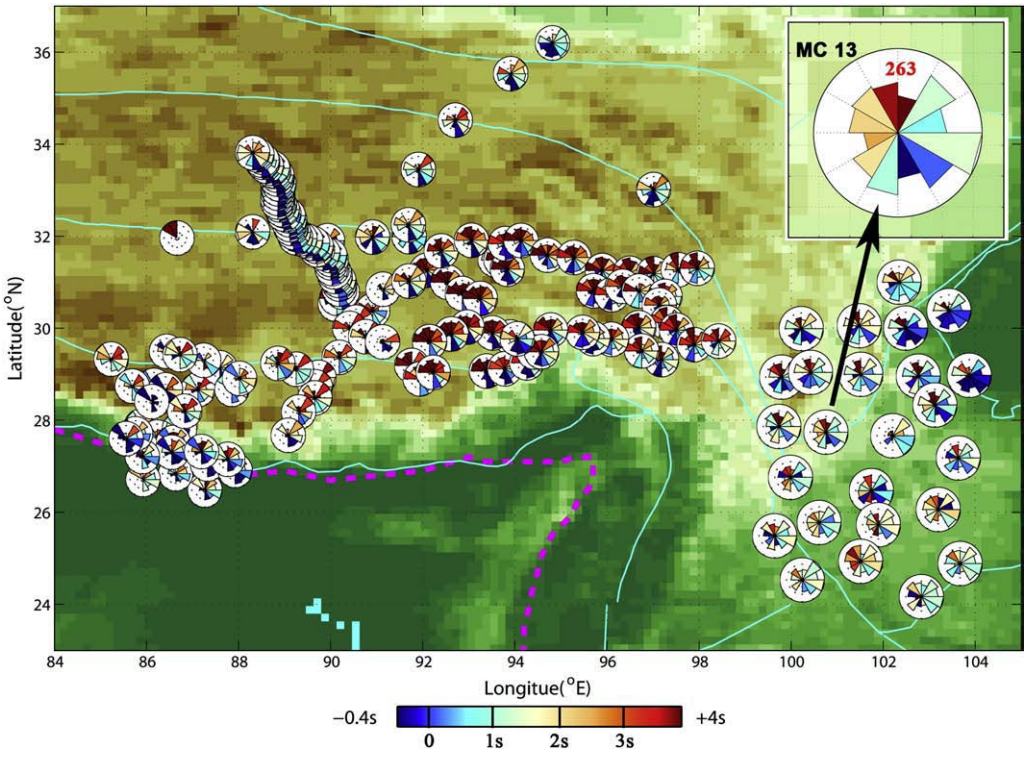

Fig. 4. Rose histograms show travel time residuals for the Tibetan arrays, after elevation correction, as a function of back-azimuth. The ~170 stations contribute a total of 35,000 arrival time picks. The inset shows one station (MC13) of the MIT-CIGMR array as an example. The red number denotes the total number of picks. (For interpretation of the references to colour in this figure legend, the reader is referred to the web version of this article.)

We use the iterative LSQR algorithm (Paige and Saunders, 1982) to minimize

$$\varepsilon = ||\mathbf{Gm}-\mathbf{d}||^2 + \lambda_1||\mathbf{m}||^2 + \lambda_2||\mathbf{Lm}||^2 + \lambda_3||\mathbf{C}-\mathbf{m_c}||^2. \quad (1)$$

Here, **m** represents the model vector, including the constant slowness perturbation in each irregular grid cell as well as hypocenter perturbation terms, **G** is the sensitivity matrix representing the sampling by the data used, and the data vector **d** represents the travel time residuals. The second and third terms represent the regularization of the solution: a large value of λ_1 puts more emphasis on minimizing the amplitude of model **m**, which biases the result toward the reference model, and λ_2 controls the smoothness of the models (**L** is a first order differential operator).

The last term in (1) is used to impose additional constraints on the model or to force a solution in a certain direction. Later we use this option to test the fit of *P* data to (scaled) *S* wave heterogeneity, but in standard applications it is used to correct for effects of crustal heterogeneity. **C** then represents an *a priori*, regional crustal model (Sun et al., 2004) which is embedded in the global model Crust 2.0 (Bassin et al., 2000), and $\mathbf{m_c}$ is the crustal part in model vector **m**. Effectively, this forces the crustal part of the model to be close to the *a priori* crust model unless the data constraints are strong enough to do otherwise. The trade-off is controlled by Lagrangian multiplier λ_3, which is determined through tests with synthetic data. This approach to crust correction is more tolerant for errors in prior crust models than methods based on explicit (static) travel time correction. Li et al. (2006) verified that with this approach the tomographic estimates of upper mantle structure do not depend significantly on the choice of crust model.

4. Results of the tomographic inversions

4.1. Image quality and resolution

Image accuracy is not easily quantified, but checkerboard tests provide at least a qualitative measure of the ability of the data to resolve the mantle structure beneath the area of interest. Travel time

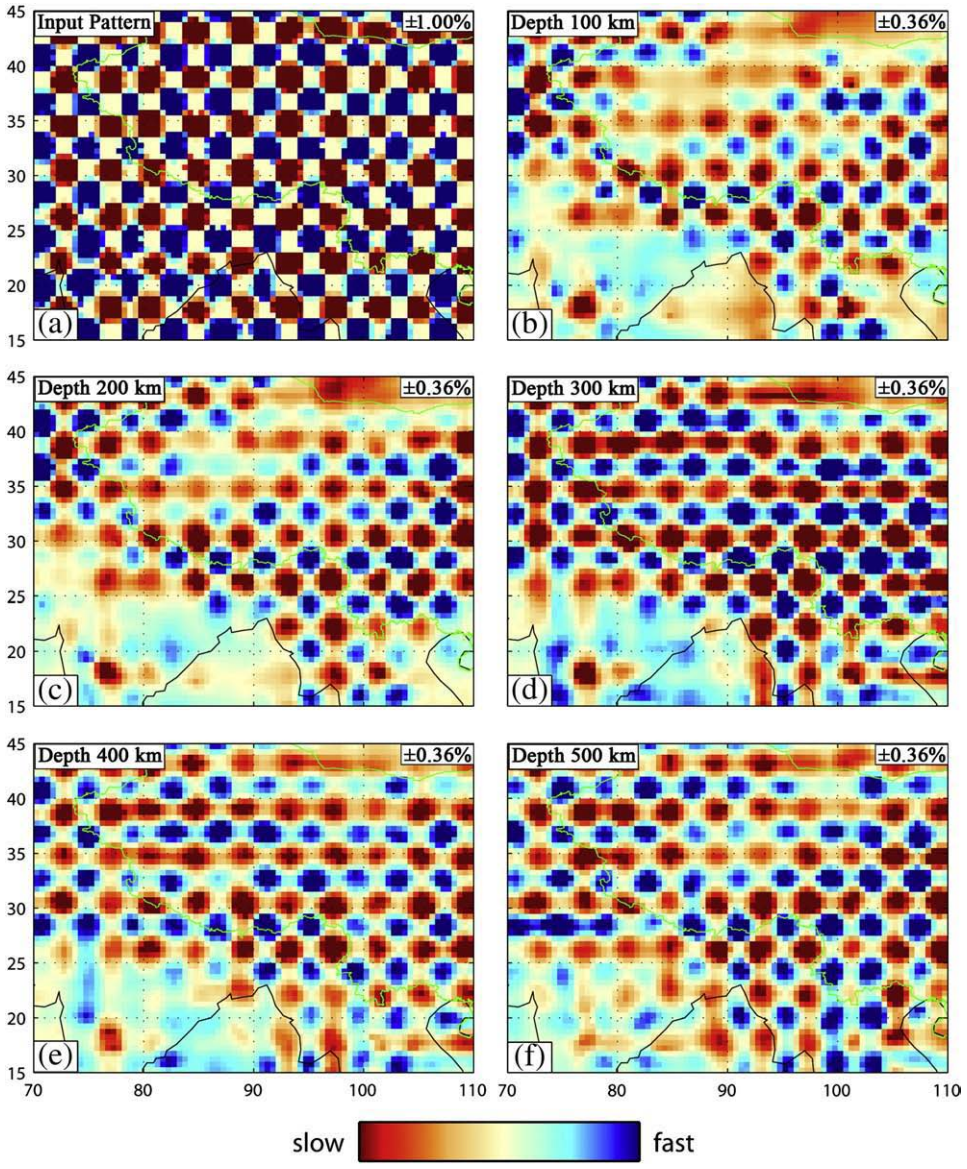

Fig. 5. Checkerboard resolution test for target anomalies at different depths as indicated in left upper corner in each subplot. The color scale is shown in the right up corner in each subplot. Input pattern (2°×2°) is shown in (a). The green line is Chinese border and the black line shows the coast line. (For interpretation of the references to colour in this figure legend, the reader is referred to the web version of this article.)

data computed for an input structure of ±1% velocity variation (Fig. 5a) were inverted using the same inversion scheme and sampling (that is, sensitivity matrix **G**) as in the inversion of observed data.

Fig. 5 illustrates the imprint of data coverage on image recovery at different depths. At 100 km depth the input anomalies are poorly recovered (or not at all) beneath Tarim basin, central India, and the Bay of Bengal, but recovery is good in the areas of our particular interest, such as the Himalayas, eastern Tibet, Sichuan Basin, and Burma (Fig. 5b). At greater depths, structure at this scale can be resolved in most of the study area. Due to regularization, only a fraction (30–50%) of the amplitude of the input signals is resolved. The real velocity anomalies in the upper mantle may thus be 2 or 3 times larger than suggested by the tomographic images, but none of the interpretations offered below are based on the absolute amplitude of the wavespeed perturbations. We also tested the ability to resolve specific target structures associated with the subduction of the Indian plate — see Electronic supplement (Fig. ES2). These tests show that resolution is variable but that the first-order features discussed below are adequately resolved.

4.2. The upper mantle beneath Tibet and surrounding regions

Fig. 6 illustrates the regional variations in *P*-wavespeed beneath Tibet and surrounding regions. To a depth of ~300 km the upper mantle wavespeeds beneath Tibet are generally (but not uniformly) slow compared to regions to the northwest (Pamirs), south and southwest (Himalayas and southwestern Tibet), and east (Sichuan and Ordos basins) of it (Fig. 6a–c). At larger depth the seismic anomalies associated with the Precambrian Sichuan and Ordos basins vanish, and the fast structure beneath the Himalayas becomes less pronounced and (laterally) more fragmented (Fig. 6d). Prominent zones of fast wave propagation appear in the transition zone beneath southwest China, central Himalayas, and Hindu Kush (Fig. 6e, f). Slow wave propagation marks the upper mantle beneath the Red River fault area

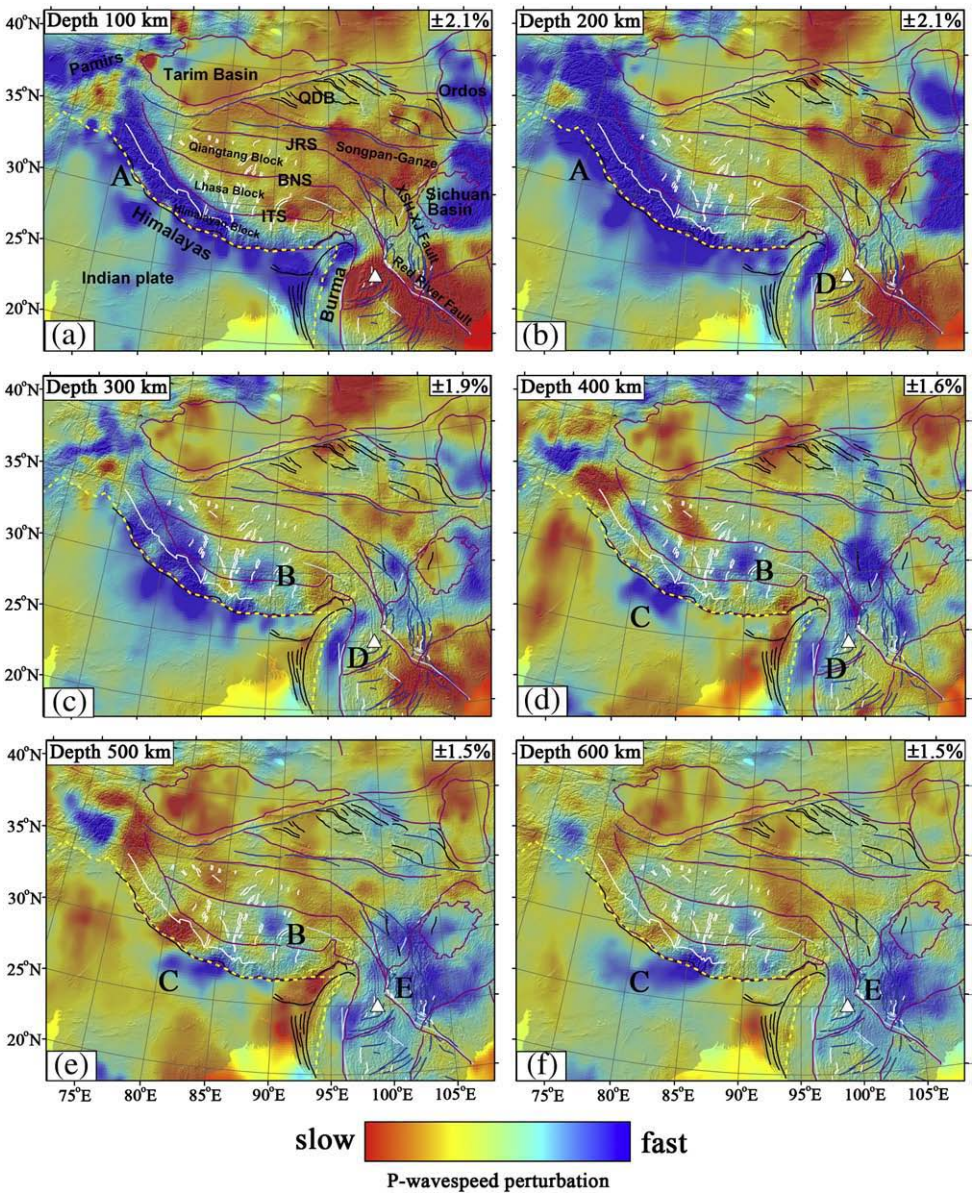

Fig. 6. *P*-wavespeed anomalies beneath Tibet and surrounding regions at different depths as indicated on the left upper corner in each subplot. Tengchong volcanic complex (white triangle) and active faults around the plateau are same as in Fig. 1. The plate boundaries (dashed yellow lines) and the block boundaries (magenta lines) are same as in Fig. 3. The significant structures have labeled as A, B, C, etc. (For interpretation of the references to colour in this figure legend, the reader is referred to the web version of this article.)

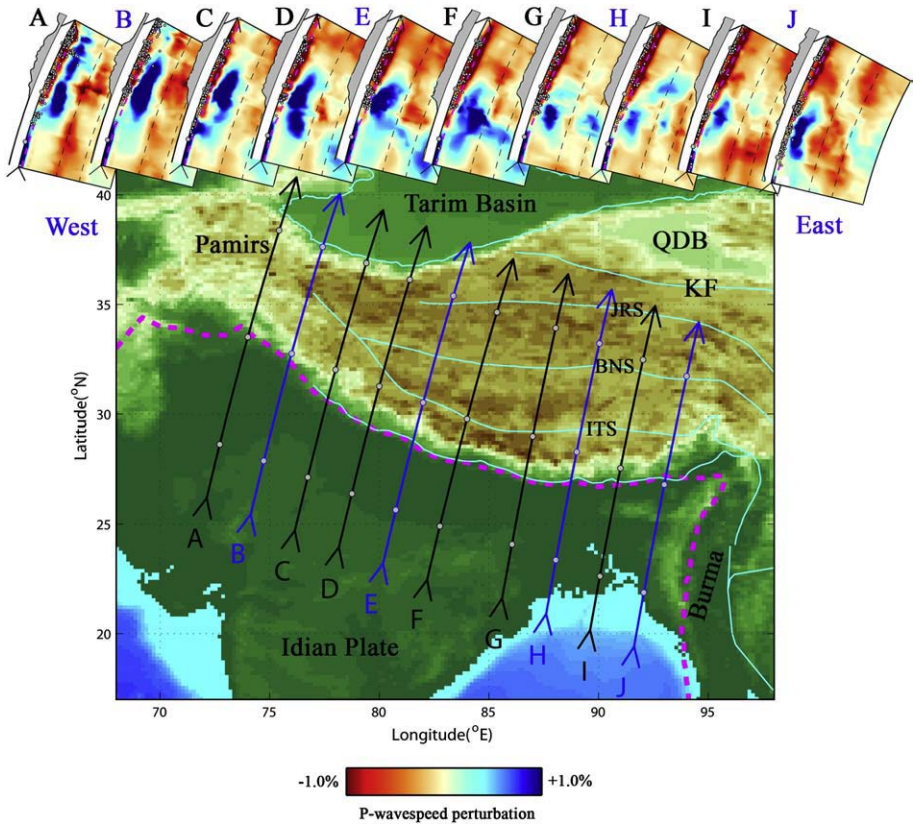

Fig. 7. Lateral variations in the Indian subduction along the collision boundary. In each cross section, gray circles are earthquakes, magenta dash lines display the Moho, gray shadow on the top of each subplot is the topography, and black dash lines are the 410 km and 660 km discontinuities. See the Electronic supplement 1 (Fig. ES1) for detail. The suture zones (ITS, BNS, and JRS) are same as in Fig. 1.

and, on a more local scale and at shallow depth (~150 km), the Tengchong volcanic complex.

4.2.1. Mantle structure beneath western and central Himalayas

Between 70 and 75°E the seismically fast structure in the mantle transition zone beneath the Hindu Kush is connected to high velocity anomalies beneath the Pamirs, which is consistent with observations by Kumar et al. (2005) and Negredo et al. (2007).

Further east, near 75°E, a high velocity anomaly structure is detected beneath the entire Tibetan plateau and reaches as far north as the western margin of the Tarim basin (structure A, Fig. 6a, b). Tests with synthetic data show that due to paucity of seismograph stations the

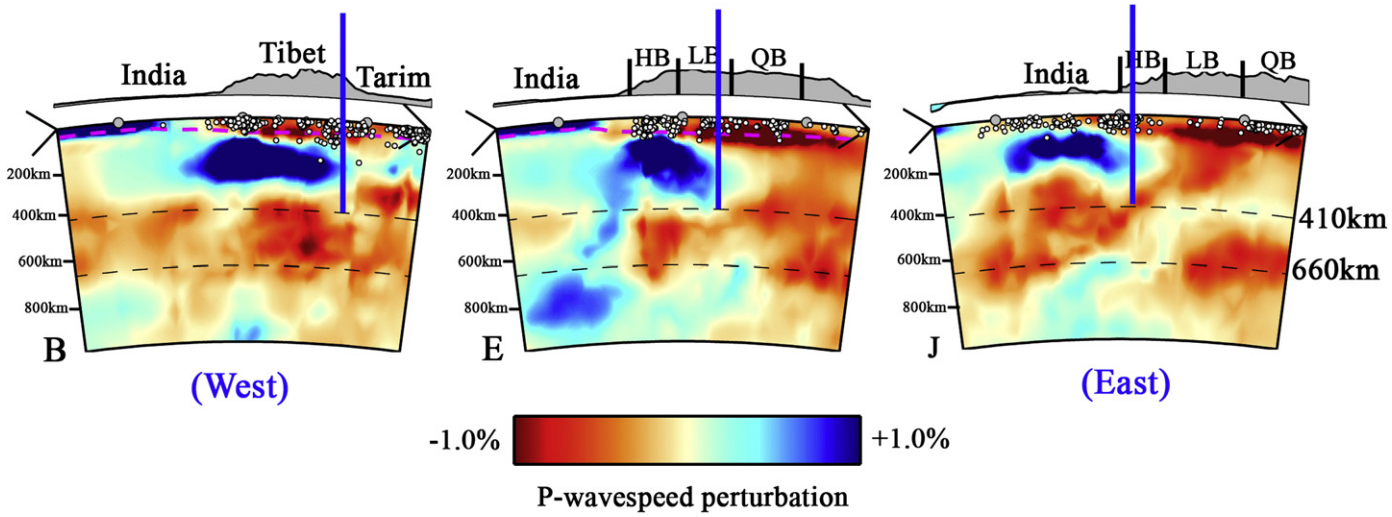

Fig. 8. The horizontal distance over which the Indian lithosphere slides northward beneath the plateau rapidly decreases from west to east. The location of the cross sections B, E, and J is shown in Fig. 7. The thick blue lines show the northern leading edge of the Indian subduction, where HB-Himalayan block; LB-Lhasa Block; QB-Qiangtang Block (Fig. 1). (For interpretation of the references to colour in this figure legend, the reader is referred to the web version of this article.)

spatial resolution is rather poor but that the fast structures beneath the plateau cannot be explained by lateral smearing of the strong anomalies beneath the Himalayas (section B, Fig. ES2).

Progressing eastward along the collision boundary, the northern extent of the fast structure beneath the Tibetan plateau, which we associate with (continental) Indian lithosphere, decreases (Fig. 7). Between 80 and 85°E there is no evidence for underthrusting of the Indian plate far beyond the Lhasa Block (section E, Fig. 8). Here the fast structure is spatially close to the high velocity anomalies in the mantle transition zone that connect to the large, fast structures (presumably formed by subducted oceanic lithosphere) in the lower mantle beneath the Indian plate (structure C, Fig. 6e, f; sections E–G, Fig. 7). The precise relationship between the shallow and deep structures cannot yet be established, but the cross sections suggest that the Indian plate has begun to override (in northward direction) the deeper, south dipping structures.

4.2.2. Mantle structure beneath eastern Himalayas

East of 85°E our tomography does not reveal prominent, seismically fast structures (in the upper 200 km of the mantle) north of the Indus–Tsangpo suture (Figs. 1 and 6a, b). Near 87–90°E the high velocity anomaly dips from the foreland basin on the Indian plate to 200–300 km depth beneath the Himalayas, and low *P*-wave velocities characterize the uppermost mantle beneath most of the Tibetan plateau (Fig. 6c). A high velocity anomaly is visible beneath the Himalayas in the lower mantle, but there is no evidence for a connection to shallow structure (section I, Fig. ES1).

Near (90°E, 31°N) moderately high velocity anomalies are visible from 300 to 500 km depth beneath the Lhasa block of Tibet (structure B in Figs. 2 and 6c–e). Resolution tests suggest that structure at this depth is well resolved and not connected to shallow mantle structure (section H, Fig. ES2).

Between 90–95°E the high velocity anomalies are confined to shallow depth beneath the foreland basin of the Indian plate and the Himalayas; these fast structures appear disconnected from the high velocity anomalies in the lower mantle (section J, Fig. 8). At this longitude there are - in our model - no prominent high velocity anomalies beneath the plateau. This is in general agreement with recent results of receiver function analysis (Oreshin et al., in press).

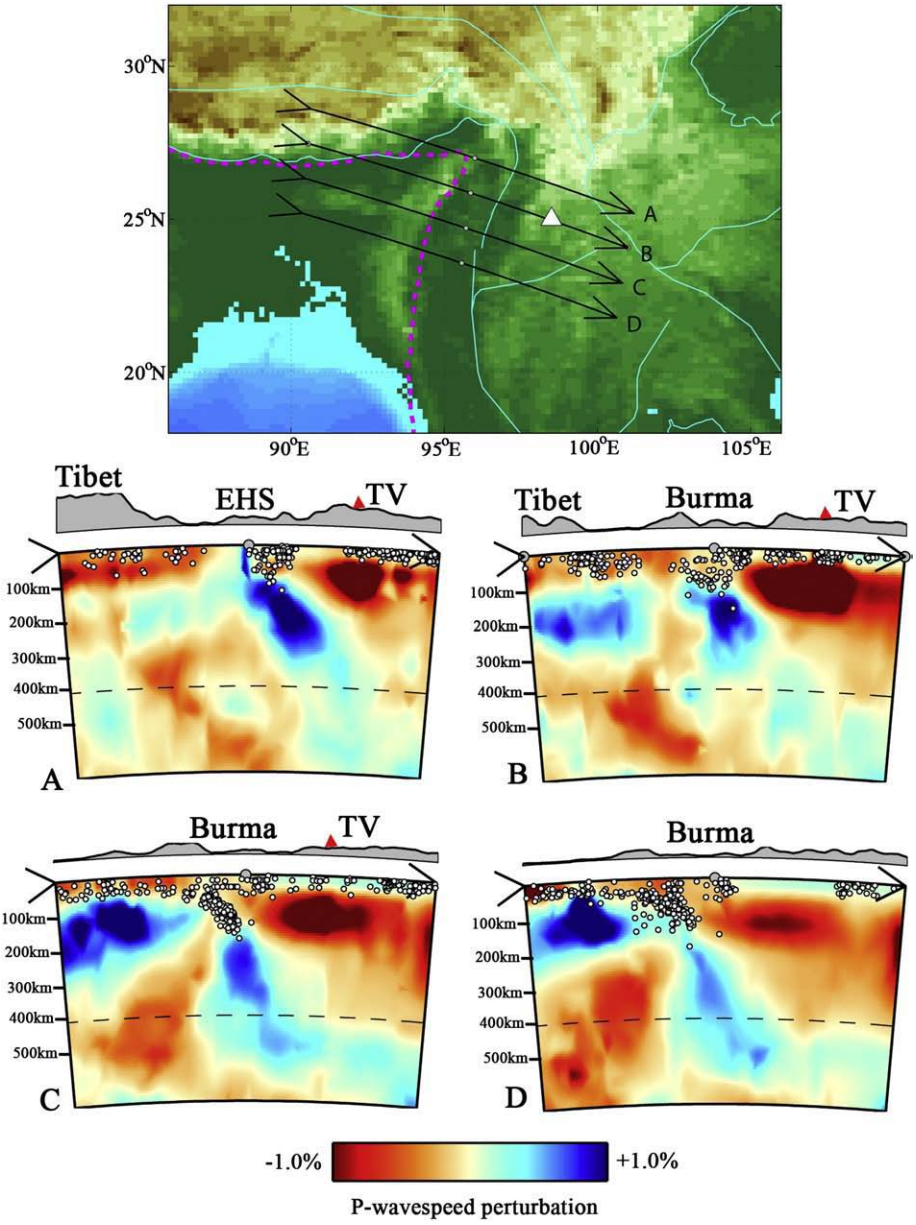

Fig. 9. *P*-wave velocity variations at four cross sections along the Burmese arc from north to south, where EHS-eastern Himalayan syntaxis, TV-Tengchong volcano.

Recent *Pn* studies (Liang and Song, 2006) also inferred average to slow *Pn* propagation in this region.

4.2.3. Mantle structure southeast of the eastern Himalayan syntaxis (EHS)

Beneath Burma, linear, seismically fast structure can be distinguished from the high velocities beneath the eastern Himalayas (structure D, Fig. 6b, c). Indeed, cross sections reveal a pronounced, east-dipping structure extending far beyond regional seismicity into the upper mantle and transition zone beneath the Indo-Burma ranges (Fig. 9). In the north it dips with an angle of ~60° to a depth of 300 km (Fig. 9A); further south it dips almost sub-vertically in the upper mantle and then spreads over a large area in the transition zone between the Burmese arc and the Red River fault (Fig. 9C, D). In the upper mantle the fast structure parallels both the shallow seismicity zone as well as the structural geological trends at the surface. However, in the transition zone beneath the Red River fault system the fast anomaly follows a northwest–southeast trend in a larger region (structure E, Fig. 6f).

The upper mantle is anomalously slow in the top 150 km of the upper mantle beneath the Tengchong volcanic complex and to greater depth beneath the Red River fault system. Eastward the latter anomaly connects to a widespread region of low seismic velocities beneath south China and the South China Sea (Fig. 6a–c). There does not seem to be a connection with the low wavespeeds beneath southeastern Tibet. In fact, in map view, the slow upper mantle beneath eastern Tibet is separated from the slow anomalies beneath the Red River by a seismically fast upper mantle structure between the Sichuan Basin and the Indo-Burma ranges. This fast anomaly extends from a depth of ~100 km to well into the transition zone (Fig. 6).

5. Discussion

The combined data from global, regional, and local seismograph networks enable high-resolution imaging of the (elastic) structure of the upper mantle beneath the Tibetan plateau, the Himalaya, and northwest Indochina. This provides new insight into the subduction of the Indian plate beneath Tibet and Burma, but it also raises new questions.

5.1. Upper mantle beneath the Tibetan plateau

Our findings of fast *P*-wave propagation in the continental lithosphere of western Tibet and low *P*-wavespeeds beneath the northernmost part of the plateau are consistent with a range of previous seismological studies. However, in view of high shear wavespeed inferred from surface wave tomography (Shapiro and Ritzwoller, 2002), the propositions of sub-horizontal underthrusting of India beneath much of Tibet (e.g., Ni and Barazangi, 1984; Powell, 1986), and the suggestion that the entire plateau could be underlain by a relatively cold lithospheric mantle (Priestley et al., 2006) it was surprising to find slow *P*-wave propagation in the upper mantle beneath most of the central and, in particular, eastern parts of Tibet (Fig. 6a, b).

In Fig. 10 we compare our *P* model (top) with the *S* model (bottom) derived from fundamental and higher mode surface wave tomography (Lebedev and van der Hilst, 2008). For this comparison we low-pass filtered our model to suppress structural details that are not resolved by surface waves, and we display the wavespeed perturbations relative to the same 1-D reference model (*ak135*, Kennett et al., 1995). At 100 km depth, the *S* model is generally consistent with our *P* model. Indeed, the long-wavelength structures surrounding the plateau (including the

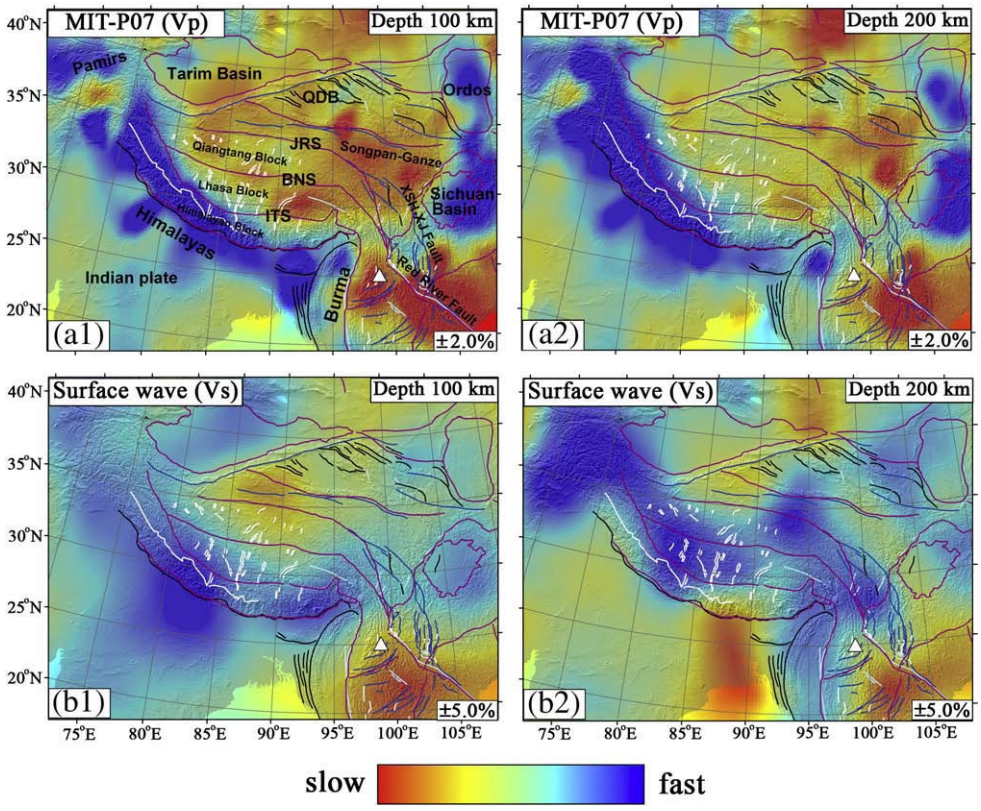

Fig. 10. Model comparison beneath the Tibetan plateau. (a1) and (a2): this study (filtered); (b1) and (b2): Shear wavespeed perturbations of model from Lebedev and van der Hilst (2008).

wavespeed anomalies beneath India, the Red River region, and the Precambrian basins east of the plateau) are remarkably similar (see also Fig. ES4a). Beneath eastern Tibet, however, shear wave propagation is neutral to fast whereas *P*-wave propagation seems to be slow. With increasing depth this discrepancy becomes more pronounced. At 200 km depth the *P*- and *S*-wavespeed perturbations beneath the plateau east of 90°E are effectively anti-correlated. We emphasize that the *P*- and *S*-wavespeeds are – generally – positively correlated away from the plateau (Fig. ES4b). The upper mantle beneath East Tibet thus seems anomalous.

Solutions of tomographic inversions are non-unique but we conducted two tests to verify that the low seismic wavespeeds are required by the *P*-wave data. In one test we inverted *P* data with a 3-D starting model derived from surface wave tomography (that is, with a pronounced fast structure beneath eastern Tibet, Fig. ES3a). For this test we used Eq. (1), above, with **C** now representing a *P*-wave model obtained by scaling from an *S*-wave model (from surface wave tomography) and with a large value of λ_3 to force the solution toward the starting model. Within a few iterations, however, the solution converges to a model with low *P*-wavespeeds beneath the plateau (Fig. ES3b), similar to the original *P* model (Fig. ES3c). In a second test we used (1) with large λ_3 to let the crust absorb as much signal as possible. For reasonable data fits, however, the resulting models still display anomalously low *P*-wavespeeds beneath eastern Tibet. These tests demonstrate that the low wavespeeds (east of 95°E) and around (90°E, 30°N) are required to fit the *P*-wave data.

The *P*–*S* discrepancy may result from differences in sampling – that is, the sensitivity to Earth's structure – by body waves and surface waves. Indeed, lateral resolution is usually better with travel time tomography whereas radial resolution is often better with surface waves (at least to a depth of 200 km or so). On the one hand, travel time inversion may overestimate the depth range where low wavespeeds prevail, even with the improved resolution of *P*-wave heterogeneity beneath east Tibet resulting from the use of data from ~170 seismograph stations of regional networks (see Fig. 5 and section B in Fig. ES2). On the other hand, surface wave tomography (with lateral resolution of ~500–1000 km) may fail to resolve a slow structure surrounded by seismically fast structures. Furthermore, some of the discrepancy could be due to seismic (radial) anisotropy and an unfortunate choice of reference values. If real, however, the discrepancy would imply (very) anomalous *Vp*/*Vs* ratios, which could perhaps reflect the presence of volatiles (e.g., water).

With these caveats in mind, and with recognition that further analysis of the *P*–*S* discrepancy is warranted, we conclude from our *P*-wave tomography that it is unlikely that a thick, cold lithosphere exists beneath central, northern, and eastern Tibet. This result agrees with Curtis and Woodhouse (1997) but seems inconsistent with Priestley et al. (2006). That the Indian plate does not, at present-day, slide far north under the central and eastern plateau corroborates the interpretation that the continental upper mantle here is not of Indian but of Asian origin (Yin and Harrison, 2000; Tapponnier et al., 2001). Further research is needed to establish if and how the anomalous upper mantle structure is causally related to the geological evolution of the eastern Tibetan plateau in the past 15 million year (Royden et al., in press).

5.2. Subduction of the Indian plate beneath the Tibetan plateau

Issues that are closely related to the nature of the upper mantle beneath the plateau, and which are of key importance for understanding the tectonic evolution of the Tibetan plateau, are (i) the lateral variations in structure and process along the collision zone and (ii) the connection – or absence thereof – between shallow structures (related to present-day processes) and deep structures (related to more ancient, presumably Mesozoic processes).

Our results suggest that underthrusting of Indian lithosphere far beneath the Tibetan plateau is restricted to the western part of the collision zone, and that the horizontal distance over which the Indian plate slides northward decreases from west to east (Fig. 8). East of ~85°E the Indian plate subducts deeper into the mantle and – as discussed in the previous section – most of the plateau proper is underlain by low velocity anomalies (Kumar et al., 2006).

From tomography with INDEPTH data, Tilmann et al. (2003) proposed that the Indian plate underthrusts the plateau as far as the Bangong–Nujiang suture (BNS) in central Tibet before plunging vertically into the mantle (Fig. 2a). We also find fast structures at ~400 km depth beneath south of the BNS (Fig. 2c), but not shallower, even though this would have been resolved by our data (section H, Fig. ES2). Instead of vertical subduction beneath central Tibet our results suggest northward dipping subduction starting at the Indus–Tsangpo suture, well south of BNS (Figs. 1 and 2c). This is consistent with the interpretation by Kosarev et al. (1999) (Fig. 2b), with slow inter-event surface wave propagation in central Tibet (Curtis and Woodhouse, 1997), and with joint inversion of *P* and *S* receiver functions that reveal low wavespeeds between 160–230 km depth beneath Lhasa and between 110–200 km near BNS (Oreshin et al., in press).

The relationship between ongoing subduction of the Indian plate and deep mantle processes associated with the subduction of ancient Tethyan lithosphere is enigmatic. Van der Voo et al. (1999) suggested that Tethyan slabs pull the Indian lithosphere into the mantle directly beneath the Indus–Tsangpo suture. Figs. 7 and 8 suggest, however, that the spatial relationship between deep and shallow slab structures varies significantly along the collision boundary. There is no evidence from our tomography for a (structural) connection beneath the western and eastern Himalayas (Fig. 8, left, right), but the relationship between shallow and deeper structure is more ambiguous beneath the central Himalayas (25–30°N, 80–87°E). The structural complexity revealed in Fig. 7e–g cannot be explained by smearing (section E, Fig. ES2). We speculate that the central Himalayas may be the only place where deep and shallow structures are still (spatially) close. But also here the (northward) subducting Indian plate may have begun to override the (south dipping) deeper part of the slab (structure C in Fig. 6d–f). While such details are, as yet, unresolved, the present-day situation may represent a late stage of slab pull from subducted Tethyan lithosphere. By implication, further India–Eurasia collision must be driven by other forces, such as (far field) ridge push and subduction of the Indian plate further west and east (e.g., along, the Sunda arc).

5.3. Subduction beneath Burma

At the corner between the Sumatra–Andaman and the Indian subduction zones, the Indo-Burma ranges are structurally complex and seismically active (to a depth of ~150 km). The Indian plate is subducting northward whereas the Burmese microplate descends eastward beneath the Eurasian plate (Ni et al., 1989). Previous tomographic studies revealed an east-dipping high velocity anomaly along the Burmese arc (e.g., Huang and Zhao, 2006). The subducted slab beneath the Burmese arc is well resolved by the data used in this study. In the northern part of this system, close to the eastern Himalayan syntaxis (EHS), the subduction is confined to the upper mantle with the dip angle of ~60° (Fig. 9A, B). In the south, the Burmese plate seems to sink into the transition zone at a dip angle that is steeper than the seismic zone (~60°) (Fig. 9C, D). The images show that at depths larger than 200 km the subduction beneath Burma is separated from subduction of the Indian plate across the EHS (structure D, Fig. 6b). Most of the subduction seems aseismic. The upper mantle part of the slab is parallel to the structural (surface) trends of the present-day arc (structure D, Fig. 6b, c), but in the transition zone it cannot be distinguished from the large, fast anomaly beneath South China (structure E, Fig. 6e, f).

The upper mantle structure may be explained by eastward subduction and westward retreat of the Burmese arc during

clockwise rotation of the Sunda block. The northeast–southwest orientation of the large, fast transition zone anomaly beneath south China (structure E, Fig. 6f) suggest that this deep structure is related to subduction along a different arc, for instance the late Mesozoic South China Trench (Honza and Fujioka, 2004). At the southwestern edge of this vast anomaly, beneath the Red River fault area, a structure with a southeast–northwest trend becomes apparent (Fig. 6f). This NW-SE trend would be consistent with the orientation of the convergent margin of south Asia prior to collision of India (Replumaz et al., 2004).

Tengchong (98°E, 25°N) is an active volcanic and geothermal complex east of the Indo-Burma arc (Fig. 1). Its most recent eruption occurred in 1609 (Qin et al., 1996). A negative gravity anomaly and high local heat flow have been used to postulate the presence of a magma chamber in the crust beneath Tengchong (Kan et al., 1996). The deeper structure of the lithosphere beneath Tengchong has not yet been well resolved (Huang et al., 2002). Our images reveal a pronounced low velocity anomaly in the shallow upper mantle beneath the Tengchong volcanic complex (Figs. 6a and 9A–C). The low velocity anomalies are confined to a depth of ~150 km, suggesting that Tengchong volcanism is related to the subduction beneath the Burmese arc. In contrast, the low velocity structure beneath the Red River fault region (Fig. 6a) continues into much greater depth (e.g., Fig. 6b–d). We speculate that this may suggest a connection between the lithospheric structure and processes beneath the Red River region and the upper mantle processes beneath Indochina, Hainan Island, and the South China Sea.

6. Conclusions

P-wavespeed variations in the upper mantle beneath the Tibetan plateau and surrounding regions have been investigated with seismic tomography using data from Tibetan arrays, CSN, and EHB.

Our observations argue against significant underthrusting of the Indian lithospheric mantle beneath the eastern plateau. By implication, most of the lithosphere beneath the central and eastern part of the plateau is of Asian origin. This interpretation is consistent with Tapponnier et al. (2001), but we do not resolve south dipping subduction zones beneath Tibet suggested by their study.

Even if the spatial resolution is not good enough to unravel the detailed structure associated with subduction of the Indian plate beneath the Himalayas, our tomography reveals significant lateral variations: subhorizontal subduction beneath the entire plateau in the west (Fig. 8, left); high velocities extending no further than the Lhasa block (LB) in central Tibet (Fig. 8, center); and underthrusting no further than the Himalayan Block (or the ITS) east of 90°E (Fig. 8, right).

In the center of the collision zone the shallow structure is either still connected to or in the process of overriding the deeper structure associated with subduction of the Tethyan slabs into the lower mantle (Fig. 8, center). In the eastern and western Himalayas our images do not provide evidence for a structural connection between present-day lithospheric structure and the deep Tethyan slabs (Fig. 8, left, right). This may suggest that the present-day situation represents a late stage in the collision controlled by slab-pull associated with Mesozoic subduction of Tethys Oceanic slabs and that collision will only continue if driven by far-field forces (e.g., subduction beneath Indochina).

At depths larger than 200 km, the subduction under Indo-Burma range appears separated from the subduction beneath the eastern Himalayas. A pronounced low velocity anomaly dominates in the top ~150 km mantle beneath Tengchong volcanic complex. Volcanism in this region is probably related to the Burma subduction. The low velocities beneath the Red River fault region extend to greater depth and may be related to the upper mantle processes further southeast.

Results from our *P* tomography are generally consistent with results from surface wave tomography but the discrepancy beneath east Tibet (fast shear wavespeed, slow *P* wavespeed) calls for further study.

Acknowledgements

We thank two anonymous reviewers for constructive comments on earlier versions of our manuscript. We are very grateful to Prof. Zhijiang Chen and his staffs at CIGMR as well as Noel Barstow from IRIS for their support and help during our field trip. We thank Dr. Freddy Aldersons to make his automatic picking software available to us. The authors have appreciated the constructive discussions with Clark Burchfiel, Leigh Royden, Barbara Romanowicz, Dan McKenzie, and Keith Priestley. This work was funded by NSF grant 6892042 of Collaborative Research in Eastern Tibet.

Appendix A. Supplementary data

Supplementary data associated with this article can be found, in the online version, at doi:10.1016/j.epsl.2008.07.016.

References

Aldersons, F., Ben-Avraham, Z., Hofstetter, A., Kissling, E., Al-Yazjeen, T., 2003. Lower crustal strength under the Dead Sea basin from local earthquake data and rheological modeling. Earth Planet. Sci. Lett. 214, 129–142.
Argand, E., 1924. La tectonique de l'Asie. Int. Geol. Congr. Rep. Sess. 13, 170–372.
Barazangi, M., Ni, J., 1982. Velocities and propagation characteristics of Pn and Sn beneath the Himalayan arc and Tibetan Plateau: possible evidence for under-thrusting of Indian continental lithosphere beneath Tibet. Geology 10, 179–185.
Bassin, C., Laske, G., Masters, G., 2000. The current limits of resolution for surface wave tomography in North America. EOS Trans. AGU 81, F897.
Besse, J., Courtillot, V., 1988. Paleogeographic maps of the continents bordering the Indian Ocean since the early Jurassic. J. Geophys. Res. 93B, 1791–1808.
Brandon, C., Romanowicz, B., 1986. A no-lid zone in the central Chang-Tang platform of Tibet - Evidence from pure path phase-velocity measurements of long period Rayleigh-waves. J. Geophys. Res. 91 (B6), 6547–6564.
Curtis, A., Woodhouse, J.H., 1997. Crust and Upper mantle shear velocity structure beneath the Tibetan plateau and surrounding regions from interevent surface wave phase velocity inversion. J. Geophys. Res. 102 (B6), 11,789–11,813.
DeMets, C., Gordon, R.G., Angus, D.F., Stein, S., 1990. Current plate motions. Geophys. J. Int. 101, 425–478.
Dewey, J., Shackleton, R.M., Chang, C., Sun, Y., 1988. The tectonic evolution of the Tibetan Plateau. In: Chang, C., Shackleton, R.M., Dewey, J.F., Yin, J. (Eds.), The Geological Evolution of Tibet. Phil. Trans. R. Soc. London, A, 327, pp. 379–413.
Engdahl, E.R., van der Hilst, R.D., Buland, R., 1998. Global teleseismic earthquake relocation with improved travel times and procedures for depth determination. Bull. Seismol. Soc. Am. 88, 722–743.
England, P., Houseman, G., 1986. Finite strain calculations of continental deformation: 2. Comparison with the India-Asia collision zone. J. Geophys. Res. 91, 3664–3676.
Friederich, W., 2003. The S-velocity structure of the East Asian mantle from inversion of shear and surface waveforms. Geophys. J. Int. 153, 88–102.
Griot, D.A., Montagner, J.P., Tapponnier, P., 1998. Phase velocity structure from Rayleigh and Love waves in Tibet and its neighboring regions. J. Geophys. Res. 103 (B9), 21,215–21,232.
Hafkenscheid, E., Wortel, M.J.R., Spakman, W., 2006. Subduction history of Tethyan region derived from seismic tomography and tectonic reconstructions. J. Geophys. Res. 111, B08401.
Holt, W.E., Wallace, T.C., 1990. Crustal thickness and upper mantle velocities in the Tibetan plateau region from the inversion of regional Pnl waveforms: Evidence for a thick upper mantle lid beneath southern Tibet. J. Geophys. Res. 95, 12,499–12,525.
Honza, E., Fujioka, K., 2004. Formation of arcs and backarc basins inferred from the tectonic evolution of Southeast Asia since the Late Cretaceous. Tectonophysics 384, 23–53.
Huang, J., Zhao, D., 2006. High-resolution mantle tomography of China and surrounding regions. J. Geophys. Res. 111, B09305. doi:10.1029/2005JB004066.
Huang, J., Zhao, D., Zheng, S., 2002. Lithospheric structure and its relationship to seismic and volcanic activity in southwest China. J. Geophys. Res. 107 (B10), 2055.
Kan, R., Zhao, J., Kan, D., 1996. The tectonic evolution and volcanic eruption in Tengchong volcanic and geothermal region (in Chinese). Seismol. Geomagn. Obs. Res. 17, 28–33.
Kárason, H., van der Hilst, R.D., 2000. Constraints on mantle convection from seismic tomography. In: Richards, M.A., Gordon, R., van der Hilst, R.D. (Eds.), History and Dynamics of Plate Motion. Am. Geophys. Union, Geophys. Monogr. Ser., 121, pp. 277–288.
Kennett, B.L.N., Engdahl, E.R., Buland, R., 1995. Constrains on seismic velocities in the Earth from travel times. Geophys. J. Int. 122, 108–124.
Kind, R., Yuan, X., Saul, J., Nelson, D., Sobolev, S.V., Mechie, J., Zhao, W., Kosarev, G., Ni, J., Achauer, U., Jiang, M., 2002. Seismic images of crust and upper mantle beneath Tibet: evidence for Eurasian plate subduction. Science 298, 1219–1221.

Kosarev, G., Kind, R., Sobolev, S.V., Yuan, X., Hanka, W., Oreshin, S., 1999. Seismic evidence for detached Indian lithospheric mantle beneath central Tibet. Science 283, 1306–1308.
Kumar, P., Yuan, X., Kind, R., Kosarev, G., 2005. The lithosphere asthenosphere boundary in the Tien Shan-Karakoram region from S receiver functions: evidence for continental subduction. Geophys. Res. Lett. 32, L07305. doi:10.1029/2004GL022291.
Kumar, P., Yuan, X., Kind, R., Ni, J., 2006. Imaging the colliding Indian and Asian lithospheric plates beneath Tibet, 23. J. Geophys. Res. 111, B06308. doi:10.1029/2005JB003930.
Lebedev, S., van der Hilst, R.D., 2008. Global upper-mantle tomography with the automated multi-mode surface and S waveforms. Geophys. J. Int. 173 (2), 505–518.
Lee, T.Y., Lawver, L.A., 1995. Cenozoic plate reconstruction of Southeast Asia. Tectonophysics 251, 85–138.
Lev, E., Long, M., van der Hilst, R.D., 2006. Seismic anisotropy in Eastern Tibet from Shear-wave splitting reveals changes in lithosphere deformation. Earth Planet. Sci. Lett. 251, 293–304.
Li, C., van der Hilst, R.D., Toks, Ö z, M.N., 2006. Constraining spatial variations in P-wave velocity in the upper mantle beneath SE Asia. Phys. Earth Planet. Inter. 154, 180–195.
Li, C., van der Hilst, R.D., Engdahl, E.R., Burdick, S., 2008. A new global model for 3-D variations of P-wave velocity in the Earth's mantle. Geochem. Geophys. Geosyst. 9, Q05018.
Liang, C., Song, X., 2006. A low velocity belt beneath northern and eastern Tibetan Plateau from Pn tomography. Geophys. Res. Lett. 33, L22306. doi:10.1029/2006GL027926.
McNamara, D.E., Owens, T.J., Walter, W.R., 1995. Observations of regional phase propagation across the Tibetan Plateau. J. Geophys. Res. 100, 22,215–22,229.
McNamara, D.E., Walter, W.R., Owens, T.J., Ammon, C.J., 1997. Upper mantle velocity structure beneath Tibet Plateau from Pn travel time tomography. J. Geophys. Res. 102, 493–505.
Molnar, P., Tapponnier, P., 1975. Cenozoic tectonics of Asia: effects of a continental collision. Science 189, 419–426.
Molnar, P., England, P., Martinod, J., 1993. Mantle dynamics, uplift of the Tibetan Plateau, and the Indian monsoon. Rev. Geophys. 31, 357–396.
Negredo, A.M., Replumaz, A., Villasenor, A., Guillot, S., 2007. Modeling the evolution of continental subduction processes in the Pamir–Hindu Kush region, E. Earth Planet. Sci. Lett. 259, 212–225.
Nelson, K.D., INDEPTH seismic team, 1996. Partially molten middle crust beneath southern Tibet: synthesis of project INDEPTH results. Science 274, 1684–1688.
Ni, J., Barazangi, M., 1984. Seismotectonics of the Himalayan collision zone: geometry of the underthrusting Indian plate beneath the Himalaya. J. Geophys. Res. 89, 1147–1163.
Ni, J.F., Guzman-Speziale, M., Bevis, M., Holt, W.E., Wallace, T.C., Seager, W., 1989. Accretionary tectonics of Burma and the three-dimensional geometry of the Burma subduction zone. Geology 17, 68–71.
Oreshin, S., Kiselev, S., Vinnik, L., Prakasam, K.S., Rai, S.S., Makeyeva, L., Savvin, Y., Crust and mantle beneath western Himalaya, Ladakh and western Tibet from integrated seismic data. Earth Planet. Sci. Lett., in press.
Owens, T.J., Zandt, G., 1997. Implications of crustal property variations for models of Tibetan plateau evolution. Nature 387, 37–43.
Paige, C.C., Saunders, M.A., 1982. LSQR: an algorithm for sparse linear equations and sparse least squares. ACM Trans. Math. Softw. 8, 43–71.
Powell, C.McA., 1986. Continental underplating model for the rise of the Tibetan Plateau. Earth Planet. Sci. Lett. 81, 79–94.
Priestley, K., Debayle, E., McKenzie, D., Pilidou, S., 2006. Upper mantle structure of eastern Asia from multimode surface waveform tomography. J. Geophys. Res. 111, B10304. doi:10.1029/2005JB004082.
Qin, J., Qian, X., Huangpu, G., 1996. The seismicity feature of the volcanic area in Tengchong (in Chinese). Seismol. Geomagn. Obs. Res. 17, 19–27.
Raphine, R., Tilmann, F., West, M., Ni, J., Rodgers, A., 2003. Crustal structure of northern and southern Tibet from surface wave dispersion analysis. J. Geophys. Res. 108 (B2), 2120. doi:10.1029/2001JB000445.
Replumaz, A., Kárason, H., van der Hilst, R.D., Besse, J., Tapponnier, P., 2004. 4-D evolution of SE Asia's mantle from geological reconstructions and seismic tomography. Earth Planet. Sci. Lett. 211, 103–115.
Rowley, D.B., 1998. Minimum age of initiation of collision between India and Asia north of Everest based on the subsidence history of the Zhepure Mountain section. J. Geol. 106, 229–235.
Royden, L.R., Burchfiel, B.C., Van der Hilst, R.D., The Geological Evolution of the Tibetan Plateau, Science (in press).
Shapiro, N.M., Ritzwoller, M.H., 2002. Monte-Carlo inversion for a global shear-velocity model of the crust and upper mantle. Geophys. J. Int. 151, 1–18.
Sol, S., Meltzer, A., Burgmann, R., van der Hilst, R.D., King, R., Chen, Z., Koons, P., Lev, E., Liu, Y.P., Zeitler, P.K., Zhang, X., Zhang, J., Zurek, B., 2007. Geodynamics of southeastern Tibet from seismic anisotropy and geodesy. Geology 35, 563–566. doi:10.1130/G23408A1.
Sun, Y., Li, X., Kuleli, S., Morgan, F.D., Toksöz, M.N., 2004. Adaptive moving window method for 3D P-velocity tomography and its application in China. Bull. Seismol. Soc. Am. 94, 740–746.
Tapponnier, P., Peltzer, G., Armijo, R., Le Dain, A., Cobbold, P., 1982. Propagating extrusion tectonics in Asia: new insights from simple experiments with plasticine. Geology 10, 611–616.
Tapponnier, P., Zhiqin, X., Roger, F., Meyer, B., Arnaud, N., Wittlinger, G., Jingsui, Y., 2001. Oblique stepwise rise and growth of the Tibet Plateau. Science 294, 1671–1677.
Tilmann, F., Ni, J., INDEPTH seismic team, 2003. Seismic imaging of the downwelling Indian lithosphere beneath central Tibet. Science 300, 1424–1427.
Van der Voo, R., Spakman, W., Bijwaard, H., 1999. Tethyan subducted slabs under India. Earth Planet. Sci. Lett. 171, 7–20.
Willett, S.D., Beaumont, C., 1994. Subduction of Asian lithospheric mantle beneath Tibet inferred from models of continental collision. Nature 369, 642–645.
Xu, L., Rondenay, S., van der Hilst, R.D., 2007. Velocity structure beneath Southeastern Tibet from teleseismic receiver functions. Phys. Earth Planet. Inter. 165, 176–193.
Yao, H., van der Hilst, R.D., De Hoop, M.V., 2006. Surface-wave array tomography in SE Tibet from ambient seismic noise and two-station analysis: I — Phase velocity maps. Geophys. J. Int. 166, 732–744. doi:10.1111/j.1365-246X.2006.03028.x.
Yao, H., Beghein, C., Van der Hilst, R.D., 2008. Surface-wave array tomography in SE Tibet from ambient seismic noise and two-station analysis: II —crustal and upper mantle structure. Geophys. J. Int. 173, 205–219.
Yin, A., Harrison, T.M., 2000. Geologic evolution of the Himalayan–Tibetan orogen. Annu. Rev. Earth Planet. Sci. 28, 211–280.
Zhao, W.J., Nelson, K.D., Project INDEPTH Team, 1993. Deep Seismic-reflection evidence for continental underthrusting beneath southern Tibet. Nature 366 (6455), 557–559.
Zhou, H.W., Murphy, M.A., 2005. Tomographic evidence for wholesale underthrusting of India beneath the entire Tibetan plateau. J. Asian Earth Sci. 25, 445–457.